DOBRE-2 WARR profile: the Earth's upper crust across Crimea between the Azov Massif and the northeastern Black Sea

V. STAROSTENKO[1]*, T. JANIK[2], R. STEPHENSON[3], D. GRYN[1], O. RUSAKOV[1], W. CZUBA[2], P. ŚRODA[2], M. GRAD[4], A. GUTERCH[2], E. FLÜH[5], H. THYBO[6], I. ARTEMIEVA[6], A. TOLKUNOV[7], G. SYDORENKO[7], D. LYSYNCHUK[1], V. OMELCHENKO[1], K. KOLOMIYETS[1], O. LEGOSTAEVA[1], A. DANNOWSKI[5] & A. SHULGIN[8]

[1]*Institute of Geophysics, National Academy of Sciences of Ukraine, Kiev, Ukraine*

[2]*Institute of Geophysics, Polish Academy of Sciences, Warsaw, Poland*

[3]*School of Geosciences, King's College, University of Aberdeen, Aberdeen, UK*

[4]*Institute of Geophysics, University of Warsaw, Warsaw, Poland*

[5]*GEOMAR, Helmholtz Centre for Ocean Research, Kiel, Germany*

[6]*Department of Geography and Geology, University of Copenhagen, Copenhagen, Denmark*

[7]*State Geophysical Enterprise 'Ukrgeofizika', Kiev, Ukraine*

[8]*Department of Geosciences, University of Oslo, Oslo, Norway*

**Corresponding author (e-mail: vstar@igph.kiev.ua)*

Abstract: The DOBRE-2 wide-angle reflection and refraction profile was acquired in June 2007 as a direct, southwestwards prolongation of the 1999 DOBREfraction'99 that crossed the Donbas Foldbelt in eastern Ukraine. It crosses the Azov Massif of the East European Craton, the Azov Sea, the Kerch Peninsula (the easternmost part of Crimea) and the northern East Black Sea Basin, thus traversing the entire Crimea–Caucasus compressional zone centred on the Kerch Peninsula. The DOBRE-2 profile recorded a mix of onshore explosive sources as well as airguns at sea. A variety of single-component recorders were used on land and ocean bottom instruments were deployed offshore and recovered by ship. The DOBRE-2 datasets were degraded by a lack of shot-point reversal at the southwestern terminus and by some poor signal registration elsewhere, in particular in the Black Sea. Nevertheless, they allowed a robust velocity model of the upper crust to be constructed along the entire profile as well as through the entire crust beneath the Azov Massif. A less well constrained model was constructed for much of the crust beneath the Azov Sea and the Kerch Peninsula. The results showed that there is a significant change in the upper crustal lithology in the northern Azov Sea, expressed in the near surface as the Main Azov Fault; this boundary can be taken as the boundary between the East European Craton and the Scythian Platform. The upper crustal rocks of the Scythian Platform in this area probably consist of metasedimentary rocks. A narrow unit as shallow as about 5 km and characterized by velocities typical of the crystalline basement bounds the metasedimentary succession on its southern margin and also marks the northern margin of the northern foredeep and the underlying successions of the Crimea–Caucasus compressional zone in the southern part of the Azov Sea. A broader and somewhat deeper basement unit (about 11 km) with an antiformal shape lies beneath the northern East Black Sea Basin and forms the southern margin of the Crimea–Caucasus compressional zone. The depth of the underlying Moho discontinuity increases from 40 km beneath the Azov Massif to 47 km beneath the Crimea–Caucasus compressional zone.

The eastern part of Ukraine, including its Black Sea domain, consists of a variety of geological structures of different ages with contrasting geodynamic origins, all located within a small area. To study the deep structure of this part of Europe, the international project DOBRE-2 was realized in 2007. DOBRE-2 consisted of wide-angle reflection and refraction (WARR) profiling, the results of which are presented here, as well as coincident near-vertical reflection profiling carried out and documented elsewhere by the Ukrainian exploration organization Ukrgeofizika and reported in part by

From: Sosson, M., Stephenson, R. A. & Adamia, S. A. (eds) *Tectonic Evolution of the Eastern Black Sea and Caucasus*. Geological Society, London, Special Publications, **428**, http://doi.org/10.1144/SP428.11

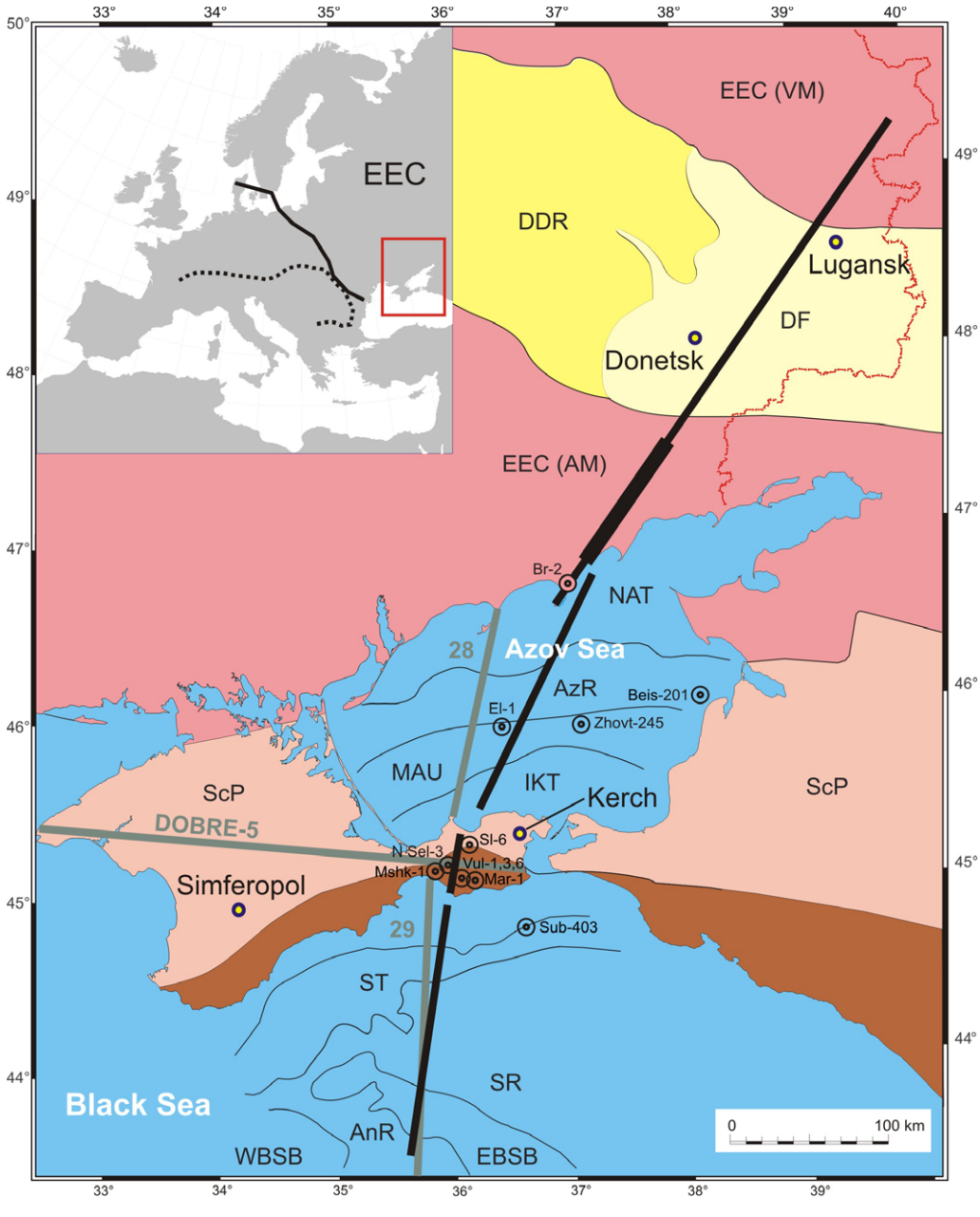

Fig. 1. Tectonic map of the study area and its location on the southern margin of the East European Craton (EEC) in a European context (red box on the inset map; the solid line marks the approximate boundary between the EEC and Phanerozoic Europe and the dotted line marks the approximate northern limit of the Alpine orogenic belt). The pink colour represents the Precambrian basement of the EEC; the darker colour is the Azov Massif (AM) and the Voronezh Massif segments (VM) and the lighter colour is the Scythian Platform (ScP) on its southern margin (e.g. Kruglov & Gursky 2007). The Dniepr–Donets rift (DDR) basin and its contiguous uplifted Donbas Foldbelt (DF) segment are coloured in dark and light yellow, respectively. The structural elements defined in the Azov Sea (NAT, North Azov Trough; AzR, Azov Ridge; MAU, Middle Azov Uplift; IKT, Indolo-Kuban Trough) are from Gerasimov *et al.* (2008). The main Crimea–Greater Caucasus compressional zone, which also lies offshore as shown, is shown in brown. Structural elements in the northeastern Black Sea (ST, Sorokin Trough; SR, Shatsky Ridge; AnR, Andrusov Ridge; WBSB and EBSB, Western and Eastern Black Sea basins, respectively) are drawn

Sydorenko *et al.* (this volume, in prep). From the NE, the DOBRE-2 profile crosses the Azov (sometimes referred to as the pre-Azov) Massif part of the Ukrainian Shield, with its exposed basement of Precambrian East European Craton, the adjacent peri-cratonic Scythian Platform and the northern margin of the Alpine–Tethys orogenic belt as expressed by the Crimea–Greater Caucasus Mountains and the eastern Black Sea (Fig. 1). The DOBRE-2 profile is a direct prolongation of the DOBREfraction'99 profile (DOBREfraction'99 Working Group 2003), with about 100 km of overlap (Fig. 1). The two profiles together form one continuous transect of length 775 km from the Voronezh Massif (the East European Craton north of the Donbas Foldbelt; Fig. 1) to the eastern Black Sea (Fig. 2).

The geological structure of the area crossed by DOBRE-2 includes tectonic features ranging in age from the Precambrian to Cenozoic (cf. Stephenson *et al.* 2004; Gozhyk *et al.* 2006; Khain *et al.* 2009). As a result of this heterogeneity and a generally poor knowledge of the deep structure and buried sedimentary layers, the deeper geology of the region remains contentious. The main purpose of the DOBRE-2 project was to image the relationship between the crust and the overlying sedimentary successions to elucidate the evolution of the sedimentary successions and the hydrocarbon systems developed within them and, in so doing, to elucidate the tectonic history of this key segment of the southern margin of the European continent.

Attempts have recently been made to determine the velocity structure in the Azov Sea and the Eastern Black Sea, in the present study area, by reconsidering legacy seismic data (DSS profile 28/29; cf. Fig. 1). The ray-tracing results of Yegorova *et al.* (2010) are not principally dissimilar to the original results based on graphical methods (Moskalenko & Malovitsky 1974). This is perhaps not surprising because the original analogue seismograms and travel-time curves from profile 28/29 now exist only on paper; recent reinterpretations are therefore based on figures and photographs from various old reports and publications. In any case, the intrinsic shortcomings of analogue recordings – such as their small dynamic range, low signal-to-noise ratio and waveform simplifications – preclude much advantage in digitizing them. Thus the DOBRE-2 WARR profile was conceived as a necessary step to obtain new insights into the crustal structure of this key geological domain.

Regional tectonic setting

There are numerous publications on the geological structure of the Black Sea region (cf. Okay *et al.* 1994; Robinson *et al.* 1995, 1996; Spadini *et al.* 1996; *Nikishin* et al. *2003*; Starostenko *et al.* 2004; Stephenson *et al.* 2004; Gee & Stephenson 2006; Gozhyk *et al.* 2006; Saintot *et al.* 2006*a*; Afanasenkov *et al.* 2007; Shillington *et al.* 2008; Khain *et al.* 2009; Khriachtchevskaia *et al.* 2010; Stephenson & Schellart 2010; Nikishin *et al.* 2011; Yegorova *et al.* 2013; Nikishin *et al.* 2015*a*, *b*; Starostenko *et al.* 2014, 2015*a*, *b*).

The DOBRE-2 profile begins on the northern margin of the Azov Massif, which is part of the Archaean–Palaeoproterozoic East European Craton; cf. Fig. 1). To the south, the Azov Sea overlies the southern margin of the East European Craton and the Scythian Platform, which is probably underlain by a younger (Proterozoic) continental fragment that accreted to the East European Craton in late Proterozoic or earliest Palaeozoic times (e.g. Gee & Stephenson 2006; Saintot *et al.* 2006*a*). There is some stratigraphic and magmatic evidence for compressional deformation of Late Triassic–Early Jurassic age in the area (Stovba & Stephenson 1999; Alexandre *et al.* 2004; Nikishin *et al.* 2011), which affected the East European Craton and Scythian Platform.

The basement structure of the Azov Sea is traditionally subdivided into a number of smaller tectonic elements (Fig. 1). These include the North Azov Trough, overlying the East European Craton basement and separated from the Azov Massif segment of the East European Craton onshore to its north by a step-like fault zone. To the south, the Azov Ridge and the Middle Azov Uplift represent basement uplifts below the northern margin of the

Fig. 1. (*Continued*) according to the Ukrgeofizika data (cf. Sydorenko *et al.* this volume, in prep). The solid black lines indicate the locations of the DOBRE-2 and DOBREfraction'99 WARR and regional CDP profiles discussed in this paper; the thicker segment is where the DOBRE-2 and DOBREfraction'99 profiles overlap. For more detail see Figure 2. The dark grey–green lines indicate the locations of the two legacy DSS lines in the offshore study area (28 and 29; cf. Yegorova *et al.* 2010) and the recently compiled and published DOBRE-5 profile (Starostenko *et al.* 2015*a*). Also shown are the locations of wells (black dots in circles with names) in the Azov Sea and northeastern Black Sea, either mentioned in the text and/or used to constrain the velocity modelling presented in this paper (Sub-403, Subbotina 403; Vul-1, Vulkanivska 1; Vul-3, Vulkanivska 3; Vul-6, Vulkanivska 6; Mshk-1, Moshkarivska 1; Mar-1, Marivska 1; N Sel-3, North Seleznivska 3; Sl-6, Slusarivska 6; El-1, Electrorozviduvalna 1; Beis-201, Beisugska 201; Zhovt-245, Zhovtneva 245; Br-2, Berdyanska 2. Cities are indicated by small, yellow-filled circles; Kerch lies on the Kerch Peninsula and Simferopol on the Crimean Peninsula.

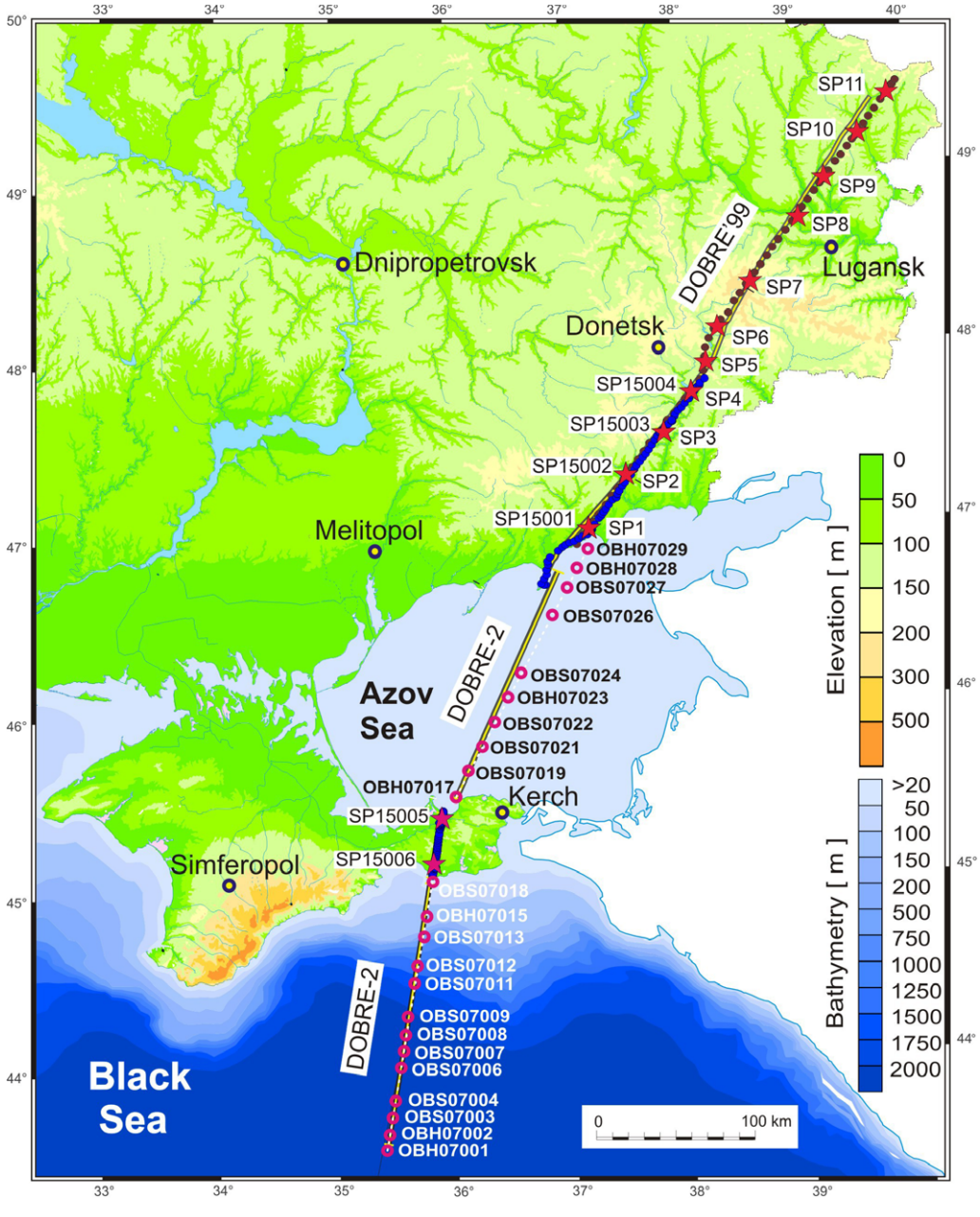

Fig. 2. Physiography and bathymetry in the study area and detailed locations of the seismic profiles discussed in this paper. Onshore receiver locations for DOBRE-2 (cf. Table 2) and DOBREfraction'99 are indicated by brown and blue dots, respectively; offshore receiver locations for the former are indicated by small red open circles connected by dashed white lines (indicating the airgun shooting line; cf. Table 1) and labelled with the recorder number (cf. Table 3). Onshore shot points are indicated by red stars, labelled SP15001–15006 and SP1–SP11 for DOBRE-2 and DOBREfraction'99, respectively. Related, near coincident, regional seismic reflection profiles are indicated by yellow-cored lines. Cities are indicated by small, yellow-filled circles; Kerch lies on the Kerch Peninsula and Simferopol on the Crimean Peninsula.

mainly Cenozoic Indolo-Kuban Trough. The Indolo-Kuban Trough consists of two separate sub-basins to the north of the Cenozoic Crimea–Caucasus compressional zone.

The Early Cretaceous and younger Black Sea Basin post-dates the early to middle Jurassic Greater Caucasus Basin that was inverted in the Cenozoic to become the present day Greater Caucasus Orogen (e.g. Saintot *et al.* 2006*b*; Nikishin *et al.* 2011). Both are believed to be back-arc basins formed mainly within strong Precambrian peri-cratonic lithosphere and in an extensional environment related to the northwards subduction of Neo-Tethys or associated oceans (Barrier & Vrielynck 2008) lying south of the study area. The regional structural architecture of the Black Sea Basin is broadly consistent with that predicted by a geodynamic model in which extension is driven by (subducted) slab rollback (Stephenson & Schellart 2010). The age and style of opening of the Black Sea's western and eastern basins, hereafter referred to as the Western and Eastern Black Sea basins (WBSB and EBSB, respectively), remain controversial given the shortage of robust data about the ages of the oldest sediments and correct information about the type of crust beneath them. Opinions range from the Jurassic to Eocene (Zonenshain & Le Pichon 1986; Okay *et al.* 1994; Vincent *et al.* 2005). Hippolyte *et al.* (2010) argued in favour of diachronous rifting in the Black Sea on the basis of new micropalaeontological age data from its inverted margin in the Turkish Central Pontides, with rifting in the WBSB starting in the Late Barremian (Early Cretaceous) and predating younger rifting in the EBSB. Nikishin *et al.* (2015*b*) concluded from new regional seismic profiles covering the whole of the Black Sea that rifting and basin formation throughout was of Cretaceous (Barremian–Santonian) age.

The northern margin of the Black Sea in general – and in this study area the northern EBSB in particular – has been strongly modified since the Eocene by compressional tectonics related to the collision of the Eurasian and Arabian plates. There is evidence of discrete inversion events in the EBSB at the end of the Middle Eocene, during the Late Eocene, at the end of the Oligocene and from the Middle Miocene to the Pliocene (Khriachtchevskaia *et al.* 2010; Stovba & Khriachtchevskaia 2011). Field observations in Crimea and the interpretation of marine common depth point (CDP) profiles suggest that the region from Dobrogea to at least the northwestern Caucasus is an inverted Early Cretaceous rift system of strongly variable configuration (Stovba & Khriachtchevskaia 2011). The main inversion zone in the study area (Fig. 1) consists of the western prolongation of the Greater Caucasus orogeny across the Kerch Shelf through to the Crimean Mountains on the southern margin of the Crimean Peninsula. In addition to this, there are numerous typical inversion features elsewhere that were formed by compression on previously normal rift faults – for example, in the Sorokin Trough on the southern margin of the main inversion zone (Fig. 1). The Andrusov Ridge (Fig. 1), part of the Mid Black Sea Rise separating the WBSB and EBSB, has resulted from inversion tectonics in a zone of earlier high amplitude normal faults formed during the Early Cretaceous Black Sea rifting, as has the Shatsky Ridge (Fig. 1) and related features forming the northeastern margin of the EBSB. Similar ages of compressional deformation have also been observed on the southern Black Sea margin and the central Pontides of Turkey (Hippolyte *et al.* 2010).

WARR data acquisition

The DOBRE-2 field acquisition programme took place in June 2007. It consisted of an onshore and offshore programme of seismic sources and recordings (Fig. 2). Onshore sources were recorded by some offshore recorders and vice versa. Details of the seismic sources are listed in Tables 1 and 2.

Onshore, 150 land seismic stations (1-component RefTek Texans) were deployed along the Azov Massif and Kerch Peninsula segments at intervals of about 1.5 and 1 km, respectively. There were six chemical explosions (600–1000 kg TNT) on land, four on the Azov Massif and two on the Kerch Peninsula (Fig. 2). The onshore shot points and corresponding shot gathers were numbered 15001–15007.

The offshore programme was carried out using two research ships, the *Iskatel* and *Topaz*. A total

Table 1. *DOBRE-2 offshore shooting programme using a 25 l airgun source*

Shot point number	Location	Latitude (°N)	Longitude (°E)	Depth (m)	Time UTC (yyyy:ddd:hh:mm:ss.sss)
SP0001–SP1187	Black Sea	44.98580–43.39827	35.83351–35.42127	−20 to −2150	2007:156:17:49:36.827 to 2007:157:14:00:45.904
SP0001–SP1085	Azov Sea	46.82666–45.43566	37.08933–36.00016	−10 to −10	2007:161:01:48:32.593 to 2007:161:20:27:14.935

Table 2. *DOBRE-2 onshore shooting programme*

Shot point number	Location	Latitude (°N)	Longitude (°E)	Height (m)	Time UTC (yyyy:ddd:hh:mm:ss.sss)	Charge (kg TNT)
SP15001	Azov Massif	46.94333	37.17611	25	2007:161:05:00:11.710	700
SP15002	Azov Massif	47.12400	37.37800	70	2007:161:06:00:04.180	800
SP15003	Azov Massif	47.52778	37.80806	95	2007:161:20:00:02.110	600
SP15005	Kerch Peninsula	45.29944	35.91417	25	2007:161:20:31:00.623	1000
SP15004	Azov Massif	47.75083	38.07250	120	2007:161:21:00:04.970	600
SP15006	Kerch Peninsula	45.04444	35.85639	5	2007:161:22:01:00.620	1000

of 23 ocean bottom seismometers (OBSs) and ocean bottom hydrophones (OBHs) were deployed in the Black and Azov seas, although one from the Black Sea was not recovered. The distance between stations was *c.* 11.25 km in the Black Sea and 14 km in the Azov Sea. Acquisition was carried out in two deployments. The first consisted of 19 OBSs and OBHs in the Black Sea (only 18 were recovered) and three in the Azov Sea. For the second deployment, 13 recorders were moved to the Azov Sea and five were left in the Black Sea (including the eventually unrecovered recorder). The recorder types, locations and depths are summarized in Table 3.

The seismic source at sea was an array of airguns with a total capacity of 25 l onboard the *Iskatel*; they were shot every 60 s on average, equivalent to about a 150–160 m interval. The total number of shots was 1187 in the Black Sea over 178 km of profile and 1085 in the Azov Sea over 173 km of profile. The shot gathers compiled for the OBSs and OBHs were numbered 07001–07028. Shooting was interrupted as necessary while operating in the Azov Sea to record ocean bottom signals from the onshore shot points.

WARR seismic data and phase correlation

Several P-wave (V_p) phases could be correlated in the seismic data and were used for modelling. Figures 3 and 4 show examples of the seismic record

Table 3. *DOBRE-2 offshore recorders*

OBH/OBS number	Location	Latitude (°N)	Longitude (°E)	Depth (m)	Recorder type
07001	Black Sea	43.42640	35.42859	2150	OBH
07002	Black Sea	43.52435	35.45276	2166	OBH
07003	Black Sea	43.62129	35.47724	2183	OBS
07004	Black Sea	43.71873	35.50252	2137	OBS
07006	Black Sea	43.91296	35.55283	2046	OBS
07007	Black Sea	44.00885	35.57782	2000	OBS
07008	Black Sea	44.10702	35.59889	1917	OBS
07009	Black Sea	44.20533	35.62520	1798	OBS
07011	Black Sea	44.39937	35.67702	1540	OBS
07012	Black Sea	44.49738	35.70317	1330	OBS
07013	Black Sea	44.69060	35.75404	660	OBS
07015	Black Sea	44.78842	35.78132	82	OBH
07018	Black Sea	44.98212	35.83265	20	OBS
07017	Azov Sea	45.45849	36.01915	10	OBH
07019	Azov Sea	45.59445	36.12379	10	OBS
07021	Azov Sea	45.73215	36.22877	10	OBS
07022	Azov Sea	45.86787	36.33333	10	OBS
07023	Azov Sea	46.00307	36.44069	10	OBH
07024	Azov Sea	46.14239	36.54835	10	OBS
07026	Azov Sea	46.45533	36.79372	10	OBS
07027	Azov Sea	46.60928	36.91596	10	OBS
07028	Azov Sea	46.72022	37.00525	10	OBH
07029	Azov Sea	46.82173	37.08685	10	OBH

OBH, ocean bottom hydrophone; OBS, ocean bottom seismometer.

sections. The seismic phases that can be easily identified and correlated include the first arrivals, representing refractions from the crustal sedimentary layers (P_{sed}), the upper–middle crystalline crust (P_g) and the upper mantle (P_n). In the later arrivals, the strongest phase is the reflection from the Moho discontinuity (P_MP). Reflections from mid-crustal discontinuities (P_cP) are also observed in some shot records. The seismic record sections show considerable variability in the wave field, reflecting differences in the tectonic structure along the profile. For most of the shot points, the first arrivals can be correlated up to *c.* 100 km offsets (P_g phase) and to about 350 km (mantle phases), as seen, for example, in Figure 3.

The P_{sed} phases are observed in the part of the profile located on the Crimean Peninsula (SP 15005–15006), with apparent V_p ranging from 2.2 to 2.5 km s^{-1} at offsets 0–15 km, increasing to 4.0–5.0 km s^{-1} in the offset range 15–45 km, suggesting a thick sedimentary succession beneath this part of the profile. In the East European Craton (the northeastern part of the profile), the P_{sed} phase is almost non-existent. Starting from the 0 km offset, the P_g phase is observed with apparent V_p of 5.5–6.25 km s^{-1}, most likely representing refractions from the crystalline basement.

Waves propagating in the upper mantle are observed for three shot points (15001, 15005 and 15006) in the offset range 180–350 km, with apparent $V = 8$–8.5 km s^{-1}. These are interpreted as refractions from below the Moho (P_n). Their late onsets (>180 km offset, 9–10 s reduced time, Fig. 3), even if this is partially caused by the substantial sedimentary thickness, suggest a deep Moho. A strong, high-velocity phase with apparent $V_p > 8.5$ km s^{-1}, observed for SP 15006 at >300 km offset, is interpreted as a reflection from a mantle discontinuity (P_1P).

Only a few reflections from crustal discontinuities are observed (e.g. SP15005 and 15006). They occur in the 20–40 km offset range and represent reflections from boundaries within the supracrustal sedimentary succession. Deeper reflected waves, interpreted as originating from the top of the lower crust, are correlated over short (*c.* 20 km) offset intervals for a few shot points only (e.g. SP 15101 and 15106). Reflections from the Moho discontinuity, sometimes hard to correlate due to relatively low signal-to-noise ratios, are observed at offsets >80 km, at *c.* 7 s reduced travel time (Fig. 4a; OBS 07013).

On the marine parts of the profile, the shallowest refractions, observed in offsets ranging from 0–1 to 0–20 km, are characterized by an apparent V_p of 1.8–2.2 km s^{-1}. The character of the deeper refracted phases allows for the determination of three areas with different uppermost crustal properties: the Black Sea, the Crimean Peninsula and the Azov Sea.

Beneath the Black Sea, the deeper refracted phase is observed in the offset range 5–10 to 20–30 km and shows an apparent V_p of 2.5–2.7 km s^{-1}. This phase is observed only at distances −420 to −280 km along the profile (OBS 07003–07012). The next observed refracted phase has an apparent V_p of 5.6–6.1 km s^{-1} and most likely represents an arrival from the crystalline basement (P_g). Between OBS 07001 and OBS 07013 this phase can be recognized at *c.* 15–20 km offset and is observed up to 30–80 km offset, depending on the signal-to-noise ratio. At OBS 07013 (Fig. 4a) it starts at 5 km offset, probably due to the shallowing of the basement horizon.

Further to the NE, beneath the Crimean Peninsula (distances 250–150 km, OBH 07017–OBS 07019), only one 3.6–3.75 km s^{-1} refracted phase is visible after the 1.8–2.2 km s^{-1} phase. Deeper refractions, including those from the basement (P_g) are not observed. Beneath the Azov Sea, starting at a distance of −170 km (OBS 07021), a basement refraction is again observed at offsets from 5 to 10 km. It occurs immediately after the shallowest, 1.8–2.2 km s^{-1} phase. At offsets up to *c.* 40 km it shows a smaller apparent velocity than in the SW ($V_p = 5.0$–5.5 km s^{-1}). In some sections (e.g. OBS 07022) it is also observed at larger offsets, up to *c.* −120 km with an apparent V_p of *c.* 6.1 km s^{-1}.

The strongest reflected phase observed in the marine data is the sea bottom reflection, together with its several multiples, best seen in the southwestern part of the profile. These multiples were useful for the detailed phase correlation as the signal-to-noise ratio is often best in the first-order multiple. Deeper phases include reflections from the boundaries between individual sedimentary layers (e.g. OBS 07006 and 07009; Fig. 4a) and a reflection from the crystalline basement (OBS07008 and 07021; Fig. 4b). In the OBS 07013 record section (Fig. 4a), reflected arrivals are observed at *c.* 11 s reduced time and in the −90 to −70 km offset range, possibly representing a Moho reflection.

Seismic modelling method and resulting P-wave velocity model

Trial and error forward modelling was carried out using the ray-tracing SEIS83 package (Červený & Pšenčík 1984) supplemented with the graphical interface MODEL (Komminaho 1998) and ZPLOT (Zelt 1994). The modelling algorithm implements ray theory and calculates ray paths, travel times and synthetic seismograms in a high-frequency approximation. The model consists of layers with smoothly varying velocities, separated

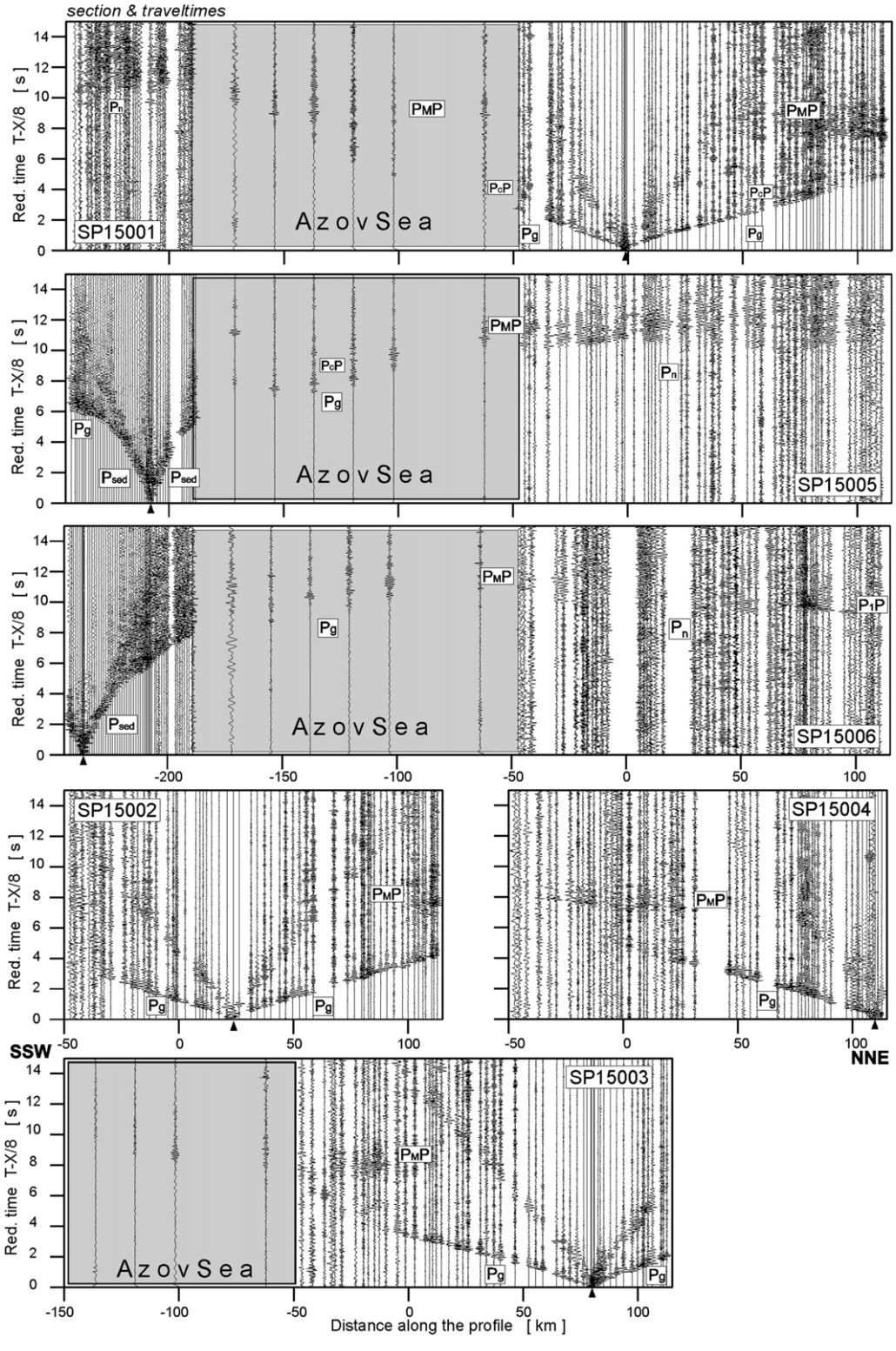

by discontinuities. In each layer, the P-wave velocity is parameterized in an irregular rectangular grid and interpolated by bicubic splines. In this study, an initial model of the uppermost crust was based on data provided by a number of previous high-resolution interpretations of seismic velocities in the area and on data from over a dozen boreholes located on or nearby the profile (cf. Fig. 1) and nearby shallow seismic reflection and refraction investigations (Khortov & Neprochnov 2006; Tsiokha *et al.* 2008; Scott 2009; Stovba *et al.* 2009; Yegorova *et al.* 2010; Gozhyk *et al.* 2011; Nikishin & Petrov 2013). Subsequently, the velocity model of the deeper layers was sought iteratively: the travel times were calculated for the initial velocity model and compared with the observed travel times. Next, the model was modified in order to minimize the misfit. The modelling also involved the calculation of synthetic seismograms and a qualitative comparison of the amplitudes of synthetic and observed data. This provided additional constraints on the velocity gradients and contrasts at velocity discontinuities. The iterations proceeded until a qualitatively satisfactory agreement between the observed and calculated travel times and amplitudes for the main phases was obtained.

The two-dimensional ray-tracing forward modelling resulted in the P-wave velocity model shown in Figure 5. Examples of the two-dimensional ray-tracing modelling of the crust for different parts of the profile are shown in Figures 6–8. The part of the profile common with DOBREfraction'99 (e.g. DOBREfraction'99 Working Group 2003), at distances of 5–110 km (Fig. 1), was modelled using data from both profiles. The seismic energy was recorded with variable quality for land shots (at offsets from 30 to 535 km) and much lower quality (at offsets up to 50 km) for the Black Sea and (up to 100 km) for the Azov Sea. As a result of the different qualities of the acquired seismic records, the derived velocity model reaches different depths along the profile. In the southern part, the data constrain the velocity model to a depth of not more than 10–14 km, in contrast with the northern part, where the model is constrained down to 40–50 km. Thanks to two long record sections from the Crimean Peninsula, SP15005 and SP15006, with relatively good quality of P_n phase arrivals and P_MP arrivals on the OBS 07013 record, it was possible to obtain information about the depth of the Moho in the −320 to −300 km and −270 to 20 km distance intervals.

Resolution analysis of the ray-tracing model

The shot times and locations of the shots and receivers were measured using global positioning system techniques to an accuracy of the order of 1 ms and tens of metres. Such errors are insignificant in a crustal-scale experiment. Uncertainties in velocity and depth in the ray-tracing model resulted primarily from the uncertainties of subjectively picked travel times, which are of the order of 0.1 s. However, the accuracy depends on the actual seismic phase correlated and changes in the quality and quantity of data (e.g. the number of shots and receivers, the effectiveness of the sources, the signal-to-noise ratio, the reciprocity of travel-time branches and ray coverage in the model).

Where the data quality was good, the ray-tracing model predicted the theoretical travel times that fitted the observed travel times for both the refracted and reflected waves with high accuracy. Several modelling tests were performed to assess this. The P-wave velocity in one crustal layer was perturbed by ± 0.2 km^{-1} with respect to the final model and the Moho depth was perturbed in the range of ± 2 km. It was clearly visible that the accuracy of the model was better than these values. Similar tests were performed, among many others, by Janik *et al.* (2002), DOBREfraction'99 Working Group (2003), Grad *et al.* (2006), Środa *et al.* (2006) and Grad *et al.* (2008). Diagrams with theoretical and observed travel times for all the phases along the profile, the ray coverage and the travel-time residuals from forward modelling are shown in Figure 9.

There is generally good agreement, with some exceptions that are not very significant. The general root mean square (RMS) misfit values are acceptable, being 0.29 for sediments, 0.18 for the crust, and 0.30 and 0.23 for the P_MP and P_n phases, respectively. The RMS misfit value for refracted phases in the crust is 0.18, whereas for reflected phases it is 0.20. The overall RMS misfit value is 0.25 from 9217 picks. The RMS misfit value for the offshore (OBS/OBH) segments is 0.26 from 8435 picks, whereas for the onshore segments it is 0.22 from 782 picks. This means that velocities in the crust, determined mainly from refracted waves, are better constrained than the depths of boundaries determined mainly from reflections. The depths of intra-crustal boundaries are determined with greater confidence than the Moho depth. The onshore segment of DOBRE-2 north of the Azov Sea is generally better than elsewhere.

Fig. 3. Examples of trace-normalized, vertical-component seismic record sections from land shots for P-waves (SP15001–SP15006) filtered by a bandpass filter (2–15 Hz). P_g, seismic refractions from the upper and middle crystalline crust; P_cP, reflections from the middle crust discontinuities; P_MP, reflected waves from the Moho boundary; P_n, refractions from the sub-Moho upper mantle; P_1P, reflections from a mantle discontinuity. The reduction velocity is 8.0 km s^{-1}.

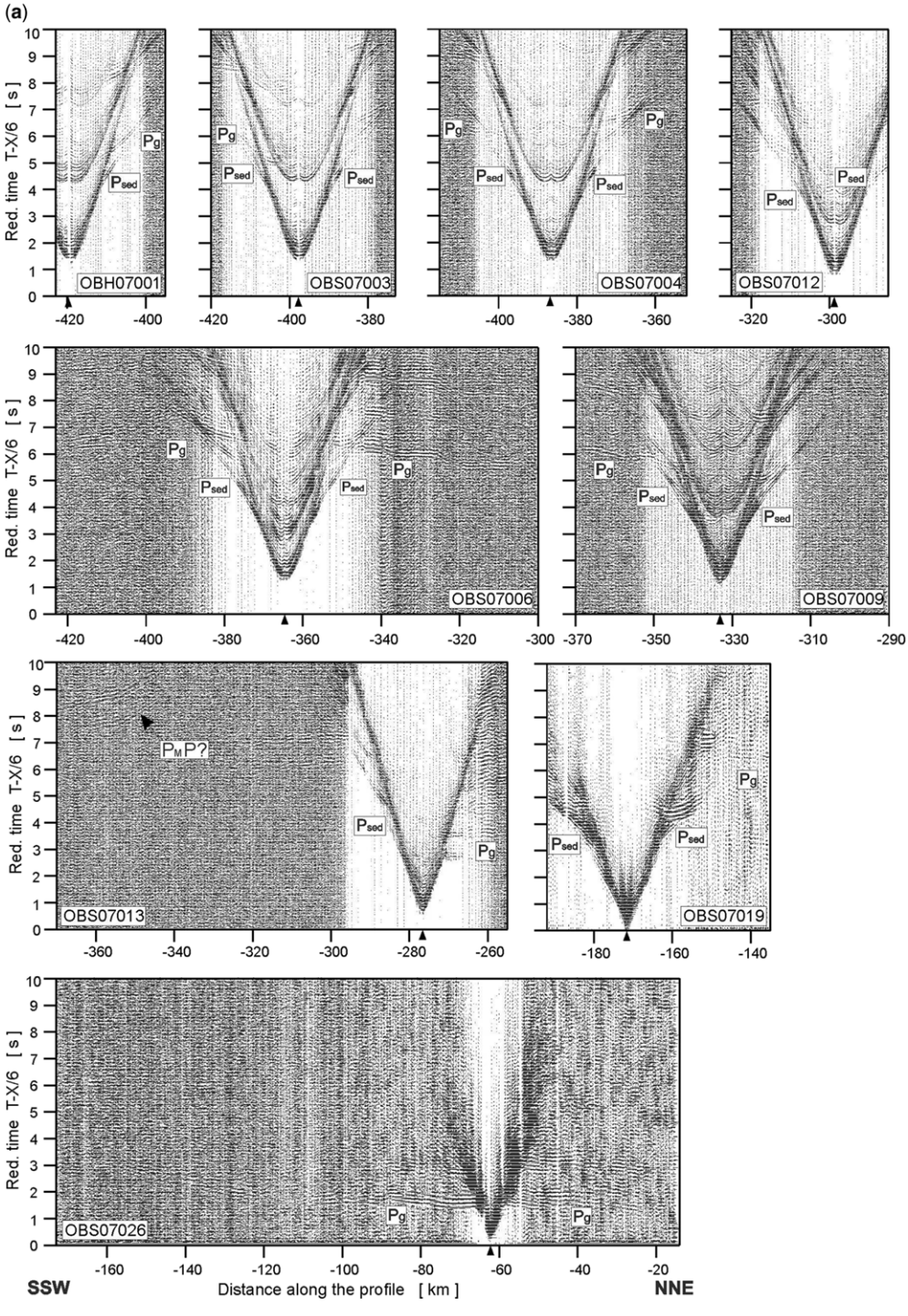

Fig. 4. Examples of vertical-component seismic record sections for (**a**) OBH07001, OBS07003, OBS07004, OBS07006, OBS07009, OBS07012, OBS07013, OBS07019, OBS07026 and (**b**) OBS07021, OBS07022, OBH07023, OBS0724 from airgun shots. P_{sed}, refractions from the crustal sedimentary layers; P_g, seismic refractions from the upper and middle crystalline crust; P_cP, reflections from the middle crust discontinuities; P_MP,

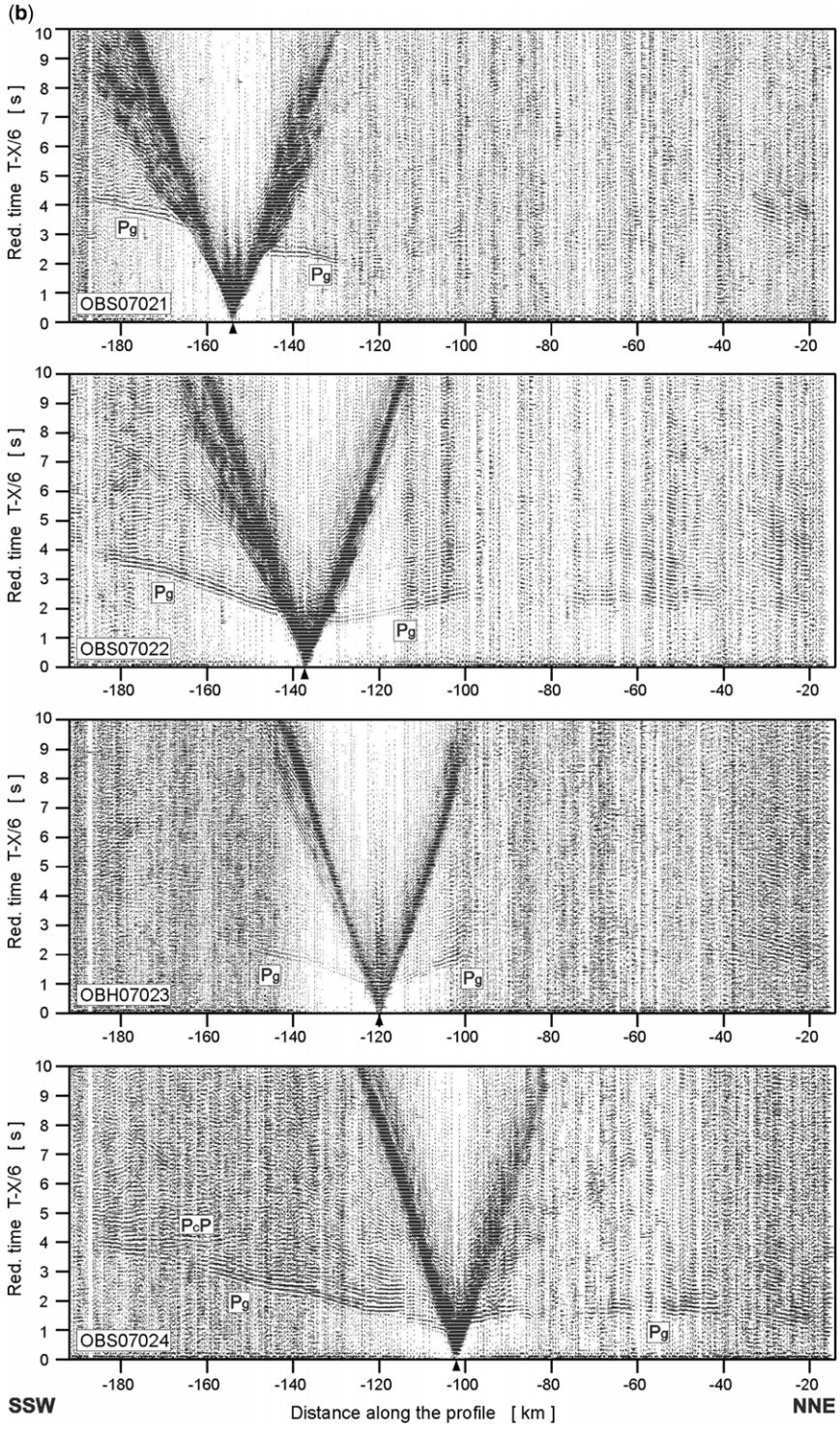

Fig. 4. (*Continued*) reflected waves from the Moho boundary; P_n, refractions from the sub-Moho upper mantle; P_lP, reflections from a mantle discontinuity. The reduction velocity is 6.0 km s^{-1}.

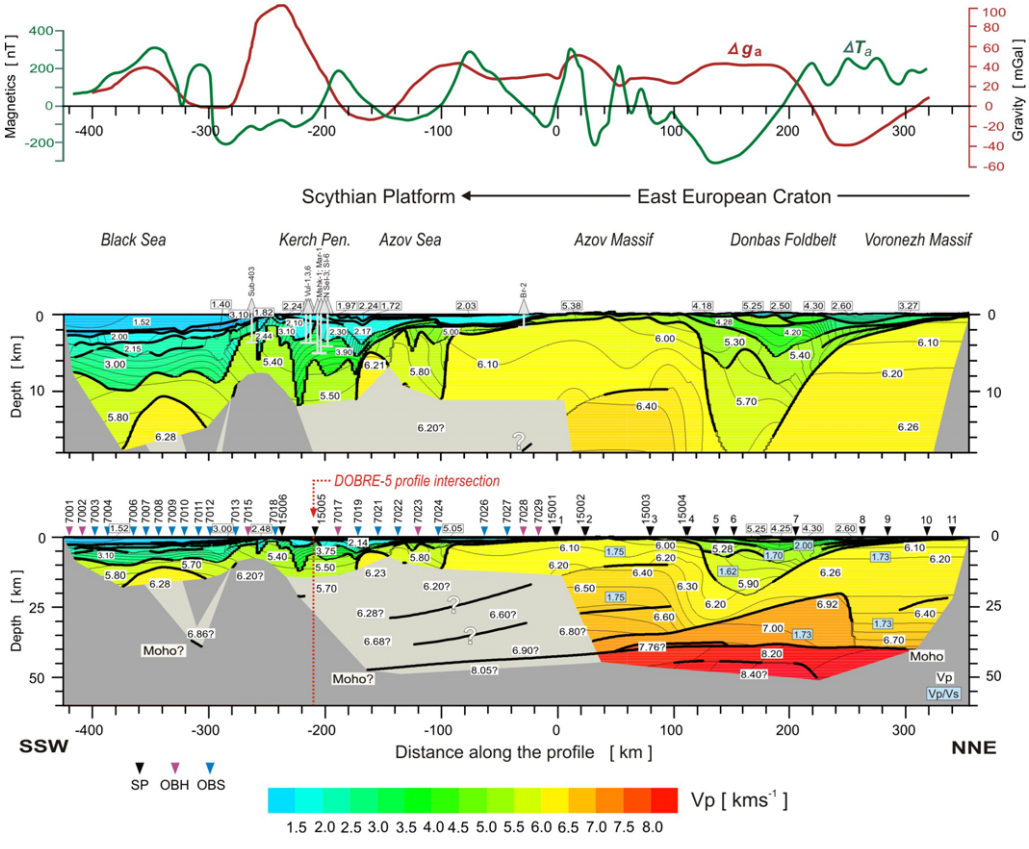

Fig. 5. Two-dimensional model of seismic P-wave velocity in the sedimentary cover (middle panel; vertical exaggeration *c.* 6.7:1) and the crust and upper mantle derived by forward ray-tracing modelling (lower panel; vertical exaggeration *c.* 2.4:1) along the DOBRE-2/DOBREfraction'99 combined transect, the latter part including the inferred P-wave to S-wave velocity ratio (V_p/V_s) on the lower panel following the model published by the DOBREfraction'99 Working Group (2003). Dark grey areas denote no ray coverage and light grey areas only limited reversed ray coverage. Boreholes (1–4.5 km deep) used for constructing an initial model for DOBRE-2 are shown as vertical grey lines, labelled with their abbreviated names as located in Figure 1. These are all within a few kilometres of the model section with the exception of Sub-403, which is about 50 km away. The black lines represent inferred major velocity discontinuities. The parts of these lines that have been directly constrained by reflected and/or refracted arrivals of P-waves are marked by thicker lines. Thin lines represent velocity isolines with values in km s^{-1} shown in white boxes. Inverted triangles on the lower panel show positions of recorders offshore (purple, OBHs; blue, OBSs; cf. Table 3) and shot points onshore (black). Gravity (Bouguer onshore and free-air offshore) and total magnetic field anomalies along the DOBRE-2/DOBREfraction'99 combined transect are shown in the upper panel (Entin *et al.* 2002; Starostenko *et al.* 2015*b*).

Discussion

The combined DOBRE-2/DOBREfraction'99 velocity model, as well as corresponding gravity and total field magnetic anomalies (Entin *et al.* 2002; Starostenko *et al.* 2015*b*) is shown in Figure 5. The magnetic anomalies are derived from air- and ship-borne surveys. The data quality and depth coverage of the velocity model are very good to excellent for DOBREfraction'99, whereas DOBRE-2 has a limited depth coverage and less data redundancy. Nevertheless, as outlined here, the DOBRE-2 model, where coverage does exist, is considered to be robust.

The DOBREfraction'99 part of the combined profile provides an excellent image of the inverted Donbas Foldbelt segment of the Late Palaeozoic Dniepr–Donets intracratonic rift basin within the Sarmatian segment (e.g. Bogdanova *et al.* 1996) of the East European Craton, including the crustal structure and Moho disposition. The >20 km thick sedimentary succession of the Donbas Foldbelt

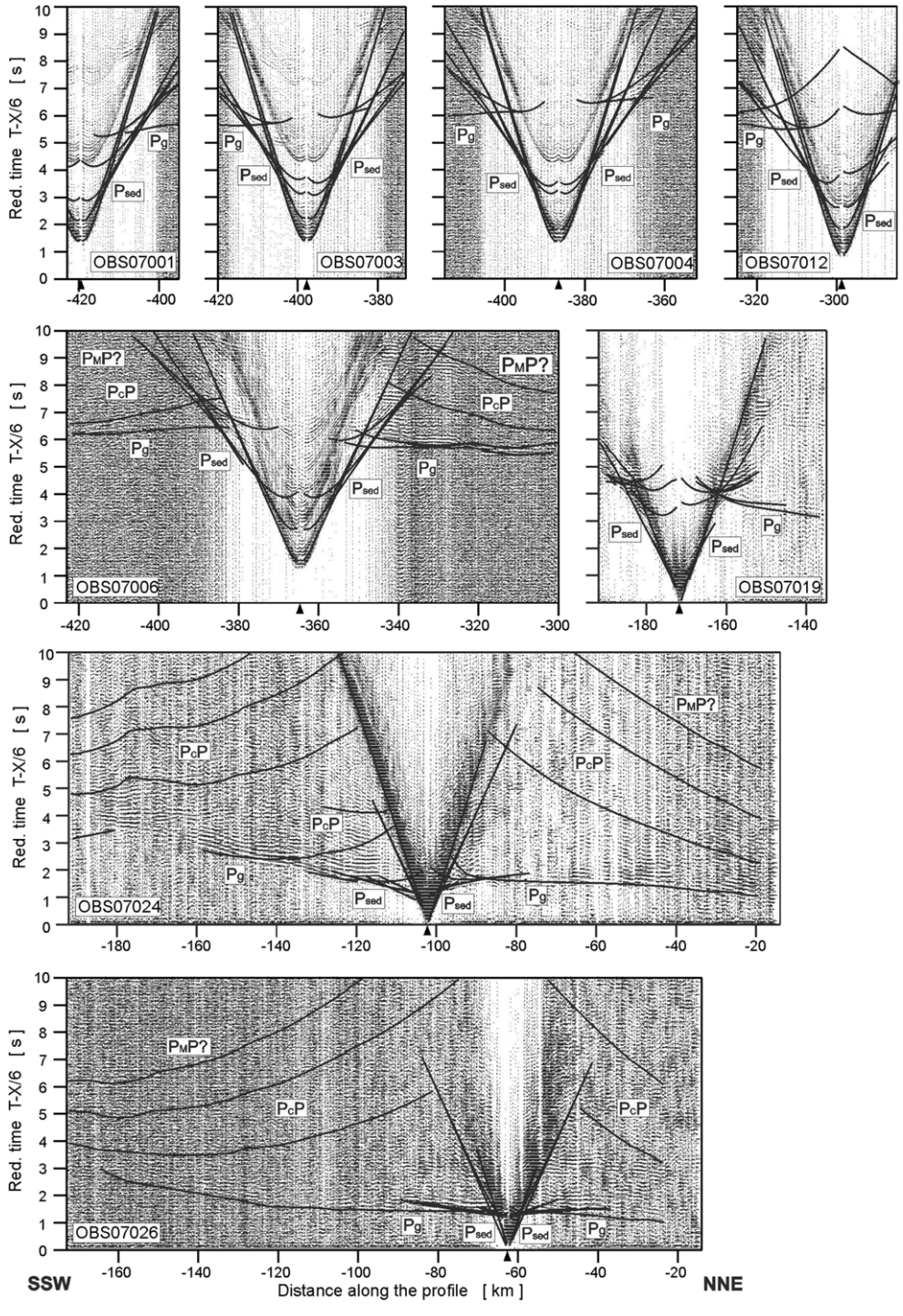

Fig. 6. Examples of model seismic phase travel times on observed record sections (as labelled). P_{sed}, refracted phases from within the sedimentary succession; P_g, refracted phases from the upper and middle crystalline crust; P_cP, reflected phases from discontinuities in the middle crust, P_MP, reflected phase from the Moho boundary; P_n, refracted phase from the sub-Moho upper mantle. The reduction velocity is 6.0 km s^{-1}.

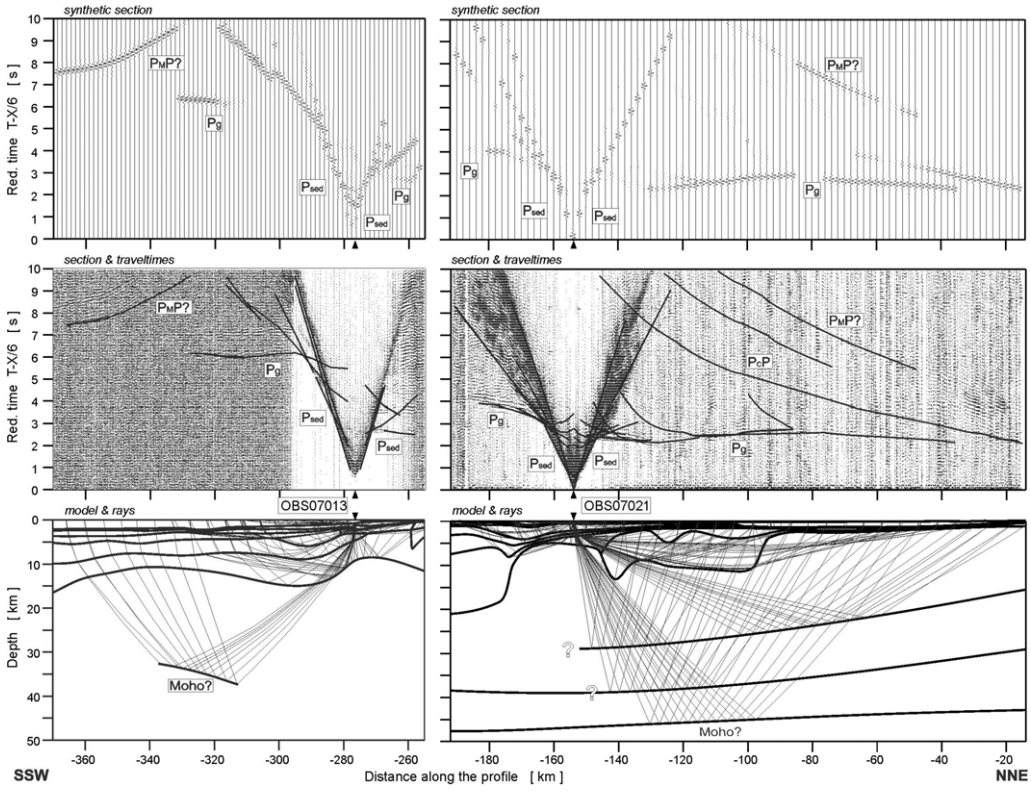

Fig. 7. Model seismic phase travel times on observed record sections OBS07013 and OBS07021 (middle panel) with corresponding ray paths (lower panel) and synthetic sections (upper panel). P_{sed}, refracted phases from within the sedimentary succession; P_g, refracted phases from the upper and middle crystalline crust; P_cP, reflected phases from discontinuities in the middle crust; P_MP, reflected phase from the Moho boundary; P_n, refracted phase from the sub-Moho upper mantle. The reduction velocity is 6.0 kms^{-1}.

consists of mainly middle to Late Devonian and Carboniferous rocks and displays velocities that are generally high for sedimentary units (up to 5.9 km s^{-1}) because of their burial and diagenesis prior to the uplift of the southern margin of the basin in the Early Permian and compressional inversion, including mild folding and uplift in the Late Cretaceous (e.g. Stovba & Stephenson 1999). Details of the DOBREfraction'99 velocity model and how it compares with its coincident deep seismic reflection profile (cf. Fig. 2) can be found elsewhere (e.g. DOBREfraction'99 Working Group 2003; Maystrenko *et al.* 2003; Stephenson *et al.* 2006; Lyngsie *et al.* 2007).

The entire East European Craton crystalline crust is incorporated into the velocity model for the overlap part of the combined DOBRE-2/DOBREfraction'99 profile (Fig. 5; cf. Fig. 1), covering the Azov Massif segment of the East European Craton. The Moho depth in this area is about 40 km. There is a suggestion in the DOBRE-2 results that the Moho depth increases by several kilometres (perhaps down to *c.* 47 km) below the Scythian Platform from the southern East European Craton boundary to the Crimea–Caucasus compressional zone, although the velocity model is relatively poorly constrained in this region below depths of 10–15 km (cf. Figs 6–8). In the southwestern part of the model, beneath the Black Sea, a possible fragment of the Moho discontinuity was modelled at a depth of about 35 km, based on P_MP arrivals (Figs 4a & 7). In this part of the model, velocities in the lower crust were assumed rather than inferred from the data.

For the most part, the DOBRE-2 only model (negative distances on Fig. 5) consists mainly of what can be interpreted as metasedimentary and sedimentary strata (P-wave velocity *c.* <5.9 km s^{-1}), exceptions being basement uplifts, both with 'domal' shapes, beneath the southern Azov Sea and the Black Sea and, most notably, the shallow (*c.* <4 km) crystalline basement inferred beneath the

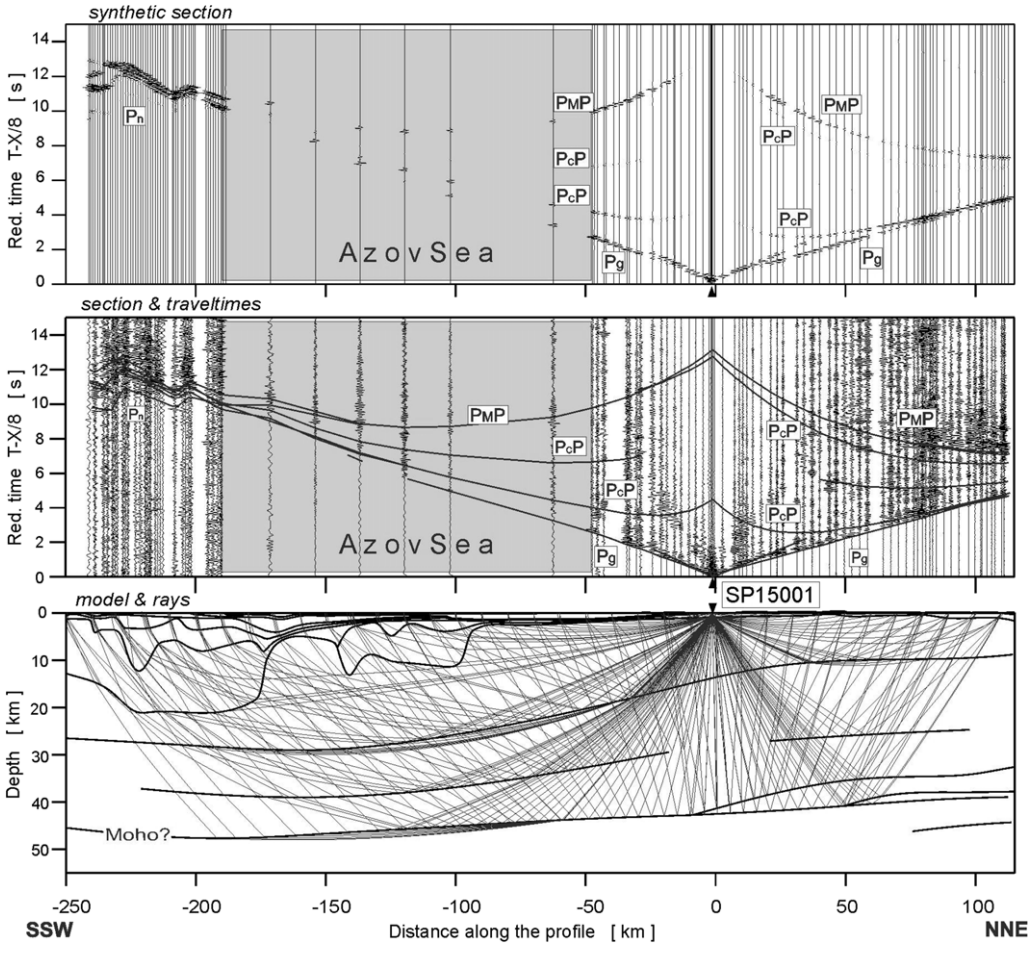

Fig. 8. Model seismic phase travel times on observed record sections for SP15001 (middle panel) with corresponding ray paths (lower panel) and synthetic section (upper panel). P_g, refracted phases from the upper and middle crystalline crust; P_cP, reflected phases from discontinuities in the middle crust, P_MP, reflected phase from the Moho boundary; P_n, refracted phase from the sub-Moho upper mantle. The reduction velocity is 8.0 km s^{-1}.

northern part of the Azov Sea (km −100 to 0), the area of the North Azov Trough; Fig. 1).

Figure 10 shows the DOBRE-2 only part of the velocity model accompanied by a geological interpretation in two-way travel time of the coincident DOBRE-2 regional near-vertical reflection profile (cf. Fig. 2). The Black Sea segment of the latter is described in more detail elsewhere in this book (Sydorenko *et al.* this volume, in prep). The geological cross-section shows how the various tectonic units mapped in Figure 1 are expressed geologically in the shallow subsurface and how this compares with the DOBRE-2 velocity model.

One important first-order inferred crustal boundary expected to lie within the crystalline crustal basement of the region crossed by DOBRE-2, although the basement is poorly and rather incompletely imaged in the DOBRE-2 velocity model, is the boundary between the East European Craton (here, its Azov Massif segment) and the basement of the Scythian Platform. The nature and possible significance of this boundary has been discussed extensively elsewhere (e.g. Sollogub 1987; Stephenson *et al.* 2004; Saintot *et al.* 2006*a*, and references cited therein). East European Craton basement rocks in the area of the velocity model are known from sampling studies to consist of Archaean–Proterozoic granitic and gneissic to migmatitic rocks (Gerasimov *et al.* 2008; Ulanovskaia *et al.* 2011). Presumed Scythian Platform basement rocks recovered from wells in the Azov Ridge–Main Azov Uplift area (wells El-1, Zhovt-245 and

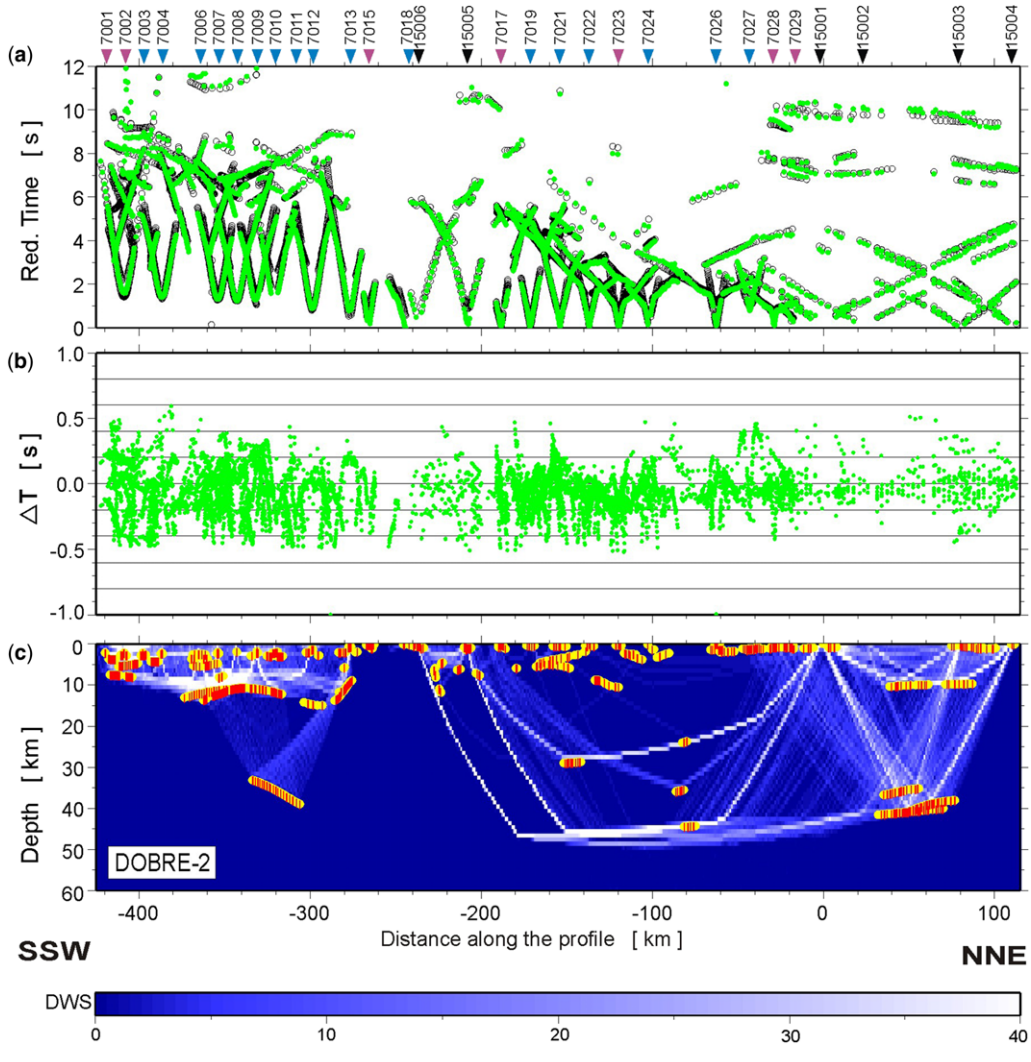

Fig. 9. (**a**) Reduced theoretical and observed travel times (reduction velocity 8.0 km s^{-1}), (**b**) travel-time residuals and (**c**) ray coverage for the presented DOBRE-2 forward modelled velocity model. Green points and black circles in (**a**) represent observed arrivals and theoretical travel times, respectively. Yellow lines in (**c**) represent fragments of discontinuities constrained by reflected phases. The red points plotted along the interfaces in (**c**) mark the bottoming points of the modelled reflected phases (every third point is plotted) and their density is a measure of the positioning accuracy of the reflectors. Ray coverage in (**c**) is illustrated by shades of derivative weight sum values, which show the relative ray density, weighting the importance of each ray segment by its distance to the node of the model.

Beis-201; Fig. 1), at depths ranging from 668 to 1631 m, consist of metamorphosed volcanogenic–terrigenous formations that are also considered to be of Precambrian age (Ulanovskaia *et al.* 2011), although there is no diagnostic faunal or radiometric age data.

In terms of the geological features mapped on Figure 1 and labelled on the cross-section in Figure 10, the North Azov Trough lies on the East European Craton basement, whereas the Azov Ridge is formed of Scythian Platform basement. The former consists of a thin, faulted layer of Mesozoic and younger sediments overlying Archaean–Proterozoic East European Craton crystalline rocks, with the latter lying below a thicker Mesozoic–Cenozoic sedimentary succession. The boundary between these two segments corresponds to the Main Azov Fault, which can, accordingly, be

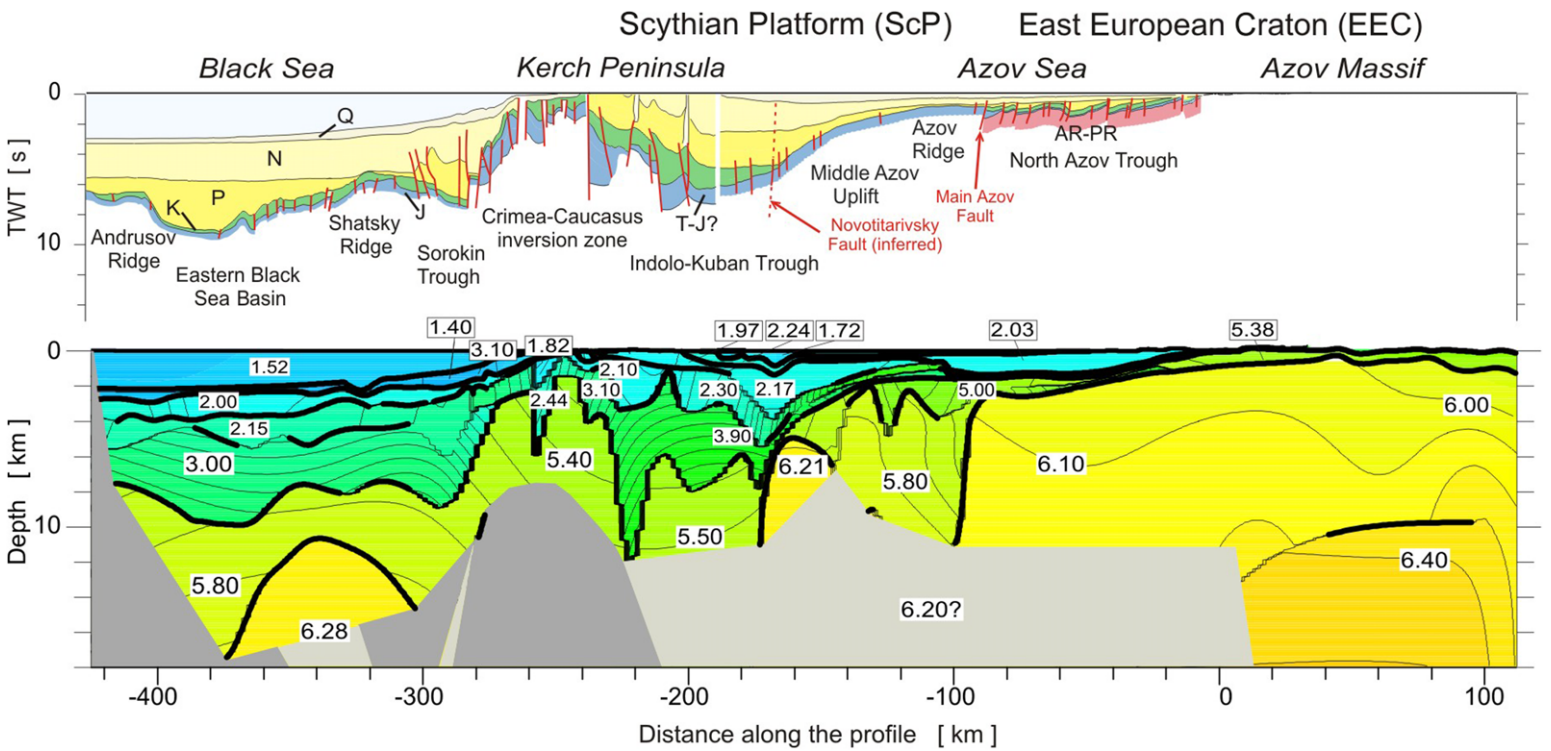

Fig. 10. The DOBRE-2 velocity model above 18 km (lower panel) and interpreted shallow geology in two-way travel time (TWT) (upper panel) from coincident DOBRE-2 seismic reflection profile (cf. Sydorenko *et al.* this volume, in prep) and other seismic and geological studies (e.g. Gozhyk *et al.* 2006; Afanasenkov *et al.* 2007; Khain *et al.* 2009; Yegorova *et al.* 2013). Structural features on the geological cross-section correspond with those in Figure 1, except for the Main Azov Fault and inferred Novotitarivsky Fault, which are mentioned in the text. P-wave velocity units are km s^{-1} with the same colour bar as in Figure 5. AR-PR, Archaean–Proterozoic; T-J, Triassic-Jurassic; K, Cretaceous; P, Palaeogene; N, Neogene; Q, Quaternary.

taken to represent at least the shallow expression of the East European Craton–Scythian Platform boundary in the Azov Sea. The velocity model in Figure 10 shows that there is also an abrupt velocity difference that can be interpreted as a deeper expression of the Main Azov Fault in this position down to at least a depth of 12 km. Velocities on the southern (Scythian Platform) side of this structure are slightly lower than on the northern (East European Craton) side and the velocity gradient has a different orientation. The 5.6–5.8 km s^{-1} velocity contours on the southern side of this structure display a fairly steep dip to the north, sub-parallel to a poorly defined, but robustly inferred, basement horizon lying to the south where velocities are >6.0 km s^{-1}.

Although the DOBRE-2 velocities inferred on the southern side of the Main Azov Fault are <6.0 km s^{-1}, somewhat less than those characterizing the East European Craton crystalline basement to the north, the borehole data suggest that the sub-Mesozoic sedimentary Scythian Platform basement also consists of Precambrian crystalline rocks, although with a different bulk lithology (of metasedimentary affinity) from that of the East European Craton. Accordingly, the Scythian Platform basement may have a different tectonic history from that of the East European Craton. It is also noted that the narrow zone of uplifted basement below the southern part of the Azov Sea (km −160) inferred in the velocity model at *c.* 6 km depth may have a velocity slightly higher than the adjacent East European Craton crust to the north. It is interpreted to represent Scythian Platform basement and, as such, is somewhat heterogeneous, of continental affinity and probably of Precambrian age.

Saintot *et al.* (2006*a*) considered the Scythian Platform to be a marginal part of the East European Craton affected by Neoproterozoic–Early Palaeozoic tectonic processes. Similarly, Gee & Stephenson (2006) suggested that the Scythian Platform basement may be part of a belt of lithosphere accreted, or at least strongly tectonically overprinted, to the northeastern and southeastern margins of the East European Craton during the Neoproterozoic. The DOBRE-2 velocity model demonstrates that the East European Craton and Scythian Platform basements, at least in the Azov Sea, have different affinities and that the latter was subject to tectonic subsidence and sedimentary basin formation in the Jurassic or earlier; however, little can be said about the underlying crystalline basement. The pre-Cenozoic sediments in this part of the Azov Sea, which are interpreted to correspond in general to velocities of 5.4–5.8 km s^{-1} in the DOBRE-2 model, are reportedly middle Triassic–Lower Jurassic argillites, interbedded with siltstones and sandstones, and Upper Jurassic limestones (Gozhyk *et al.* 2006; Ulanovskaia *et al.* 2011). Sediments displaying similar velocities in the Black Sea are interpreted as Upper Jurassic limestones (Robinson *et al.* 1995), thought to be part of a single 'Neo-Tethyan' carbonate platform in this region (Nikishin *et al.* 2011).

The units to the south of the 'domal' Scythian Platform basement unit (V_p = 6.21 km s^{-1}) centred around km −160 are interpreted as (meta)sedimentary (velocities *c.* 5.4–5.7 km s^{-1}) and may be as thick 20–22 km based on the short 5.7 km s^{-1} boundary at km −220 seen in Figure 5 (lower panel). The boundary between these metasedimentary units and the Scythian Platform basement unit to their north is very steep and its position coincides approximately with the location of the inferred Novotitarivsky Fault (Gozhyk *et al.* 2006; Khain *et al.* 2009). This roughly east–west-trending fault is traced to a depth of about 11 km in the DOBRE-2 velocity model (Fig. 10). It may be deeper (20–23 km) according to other interpretations of deep seismic sounding data in the area and has been traditionally considered as the northern limit of the western Indolo-Kuban Trough (Kerimov 2004; Panina 2009). The DOBRE-2 velocity model supports the existence of such a deep structure and that it is indeed a sedimentary basin bounding fault; the sedimentary basin formed on Scythian Platform basement and is therefore younger than this basement. The southern margin of the inferred deeply buried 'sedimentary basin' is the basement uplift at *c.* 10–11 km depth beneath the Shatsky Ridge of the northern Black Sea (km −340), with the implication that this unit also consists of Scythian Platform basement. This is in accordance with local tomography models of the area, which have been interpreted as indicating that basement in this area could also be of Scythian Platform basement affinity (Gobarenko *et al.* 2015).

According to the DOBRE-2 velocity model, the Moho depth increases from 40 km beneath the Azov Massif to about 47 km in the area of the inferred Novotitarivsky Fault (km −170), possibly reflecting the flexural effects of loading by the Indolo-Kuban Trough in its foredeep setting with respect to the main Crimea–Caucasus compressional zone. The DOBRE-2 model Moho depth in this area is supported by the results of the east–west-oriented DOBRE-5 profile, which crosses DOBRE-2 on the Kerch Peninsula (cf. Fig. 5; km −210) and shows a Moho depth of 47–48 km (Starostenko *et al.* 2015*a*). The DOBRE-5 velocity model reports velocities <6 km s^{-1} down to a depth of about 15 km, consistent with the sedimentary layer inferred on the DOBRE-2 model to its depth limit of 10–11 km. The intervening crystalline crustal layer in DOBRE-5 has velocities of 6.8–6.9 km s^{-1}, also similar to what is tentatively inferred in the neighbouring Azov Sea segment of the DOBRE-2 model.

The gravity and magnetic anomalies shown in Figure 5 are broadly in agreement with the DOBRE-2 velocity in this area. The main gravity high along the profile, centred at about km −240, roughly corresponds with the axis of the Crimea–Caucasus compressional zone in the vicinity of the Kerch Peninsula, indicative of the higher velocity (and denser) rocks uplifted into shallower structural levels below the inversion axis. The view that these are sedimentary rocks of an older, deeply buried sedimentary basin, as suggested, is supported by the absence of a magnetic anomaly in the same region. In contrast, where the velocity model depicts what are interpreted here as basement uplifts north and south of the inversion zone (km −160 and km −340), there are approximately coincident magnetic highs suggestive of shallower basement in these areas.

However, whatever the crystalline basement is in the area south of the Azov Sea, it has been highly disturbed, presumably intruded and deformed, during the Mesozoic (and possibly early Cenozoic) formation of the Eastern Black Sea and the subsequent period of compressional tectonism leading to the Crimea–Caucasus compressional zone crossed by DOBRE-2 north of the EBSB. These tectonic events, and possibly earlier events, have shaped the heterogeneous architecture of the sedimentary successions imaged more clearly and more completely in the DOBRE-2 velocity model. In general, it is suggested that those successions characterized by velocities of 4.5–5 km s^{-1} and less may be associated with extension of the Black Sea and the inversion stages of sedimentary basin formation, whereas those with velocities higher than this (up to *c.* 5.8–5.9 km s^{-1}) may be indicative of earlier tectonic settings, although this cannot be said with certainty.

Summary and conclusions

The DOBRE-2 WARR profile crosses the Azov Massif, the adjacent Scythian Platform and the northern margin of the Alpine–Tethys orogenic belt, the last as expressed by the Crimea–Greater Caucasus compressional zone and the contiguous Azov Sea and northern part of the eastern Black Sea. The DOBRE-2 profile is a direct prolongation of the DOBREfraction'99 profile (cf. DOBREfraction'99 Working Group 2003), together forming one continuous transect of 775 km length.

The DOBRE-2 WARR data, consisting of a number of shot gathers from onshore shot points as well as numerous OBH and OBS records in the Azov and Black seas, were modelled using a ray-tracing method. The resulting velocity model is well constrained to uppermost mantle depths beneath the Azov Massif (and contiguous crustal segments covered by DOBREfraction'99) and within the upper crust (to a depth of 10–15 km) beneath the Azov Sea, Kerch Peninsula and northern part of the EBSB. The data provide some coverage of the entire crust beneath the Azov Sea area.

The main results are as follows. There are two velocity domains that are interpreted to consist of sedimentary or metasedimentary successions, characterized by velocities in the ranges 1.8–3.9 and 5.4–5.8 km s^{-1}, respectively. These overlie a 6.2–6.8 km s^{-1} layer that represents the crystalline crust. The depth of the underlying Moho discontinuity increases from 40 km beneath the Azov Massif to 47 km beneath the Crimea–Caucasus compressional zone.

This generally shallower sedimentary domain (e.g. 1.8–3.9 km s^{-1}) is thickest on either side of the Crimea–Caucasus compressional zone centred on the Kerch Peninsula and is interpreted to consist primarily of sedimentary rocks of Mesozoic and younger age deposited during the extensional tectonic phase dominated by the formation of the Black Sea (mainly Cretaceous–Paleocene) and during the subsequent compressional phase of Crimea–Caucasus deformation (Eocene and younger).

The generally deeper sedimentary domain (5.4–5.8 km s^{-1}) is interpreted to consist primarily of highly indurated sedimentary rocks of (Mesozoic–) Palaeozoic and older age. This layer is thin below the northern part of the Azov Sea and on the Azov Massif (or, indeed, absent with the shallowest velocity unit in this area being $<$5.4 km s^{-1}) and thickens abruptly in the area of the Main Azov Fault, which is mapped in the Azov Sea by shallow seismic studies. This is imaged in the velocity model by a decrease in lateral velocity from 6.0–6.2 km s^{-1} (crystalline crustal basement) to 5.6–5.8 km s^{-1} (metasedimentary rocks) to a depth of 12 km, interpreted to be the deeper expression of the Main Azov Fault and indicating a southerly dip of this fault of about 40°. This structure can be taken as the boundary between the crust of the East European Craton (Azov Massif) to the north and the crust of the Scythian Platform to the south.

The metasedimentary rocks of the Scythian Platform south of the Main Azov Fault are thought to be of Precambrian age based on geological evidence and they are bounded to the south by an uplift of crystalline basement (e.g. 6.2–6.8 km s^{-1}) to a depth of about 6 km. A substantial (14 km) and sharp deepening of the 5.4–5.8 km s^{-1} layer marks the southern limit of the inferred uplift of the crystalline basement and corresponds to the position of the inferred Novotitarivsky Fault, which has been considered to be the northern limit of the mainly syn-compressional (foredeep) Indolo-Kuban Trough. Its deeper expression, as seen in the DOBRE-2 velocity model, indicates the possibility

of an older sedimentary succession underlying the younger Indo-Kuban succession.

An antiformal 'uplift' of crystalline basement to about 11 km is inferred beneath sedimentary successions underlying the Shatsky Ridge area of the northern EBSB. A velocity of 6.28 km s^{-1} is inferred for the basement rocks in this area, not dissimilar to that of the northern margin of the Indolo-Kuban Trough and deeper sedimentary successions (6.21 km s^{-1}).

The fieldwork and data acquisition along the DOBRE-2 profile were carried out as an international collaboration. The authors sincerely thank the many people and organizations from Ukraine, Denmark, Germany, Poland and the Netherlands who contributed to DOBRE-2, especially the technical experts during the field expedition. We express our gratitude to their staff for technical support as well as to the crews of the ships *Iskatel* and *Topaz*, who actively participated in the offshore operations. The authors also thank the chief editor of this Special Publication, Marc Sosson (University of Nice Sophia Antipolis, France) and two reviewers – Randy Keller (University of Oklahoma, USA) and an anonymous reviewer – for helpful comments and suggestions. This work was partly supported within statutory activities No. 3841/E-41/S/2014 of the Ministry of Science and Higher Education of Poland. RS acknowledges support from the Royal Society of Edinburgh for facilitating the collaboration that has led to the production of this manuscript. The public domain GMT package (Wessel & Smith 1995) was used to produce some of the maps.

References

Afanasenkov, A. P., Nikishin, A. M. & Obukhov, A. N. 2007. *Eastern Black Sea Basin: Geological Structure and Hydrocarbon Potential*. Scientific World Publishing House, Moscow [in Russian].

Alexandre, P., Chalot-Prat, F. *et al.* 2004. The $^{40}Ar/^{39}Ar$ dating of magmatic activities in the Donbas Foldbelt and the Scythian Platform (Eastern Europe an Craton). *Tectonics*, **23**, TC5002, http://doi.org/10.1029/2003TC001582

Barrier, E. & Vrielynck, B. 2008. *Palaeotectonic Maps of the Middle East. Tectono-sedimentary-palinspastic Maps from Late Norian to Piacenzia. Atlas of 14 Maps, Scale 1/18 500 000*. Commission for the Geological Map of the World (CGMW/CCGM)/UNESCO, http://www.ccgm.org

Bogdanova, S. V., Pashkevich, I. K. *et al.* 1996. Riphean rifting and major Palaeoproterozoic crustal boundaries in the basement of the East European Craton: geology and geophysics. *Tectonophysics*, **258**, 1–21.

Červený, V. & Pšenčík, I. 1984. SEIS83 – Numerical modelling of seismic wave fields in 2-D laterally varying layered structures by the ray method. *In*: Engdahl, E. R. (ed.) *Documentation of Earthquake Algorithms*. World Data Center for Solid Earth Geophysics Report SE-35, 36–40.

DOBREFRACTION'99 WORKING GROUP 2003. 'DOBREfraction'99' – velocity model of the crust and upper mantle beneath the Donbas Foldbelt (East Ukraine). *Tectonophysics*, **371**, 81–110.

Entin, V. A., Shumkiv, L. M. *et al.* 2002. *Preparing the Geophysical Basis for a Tectonic Map of Ukraine of 1: 1000000 Scale*. Geoinform of Ukraine, Kiev [in Ukrainian].

Gee, D. G. & Stephenson, R. A. 2006. The European lithosphere: an introduction. *In*: Gee, D. G. & Stephenson, R. A. (eds) *European Lithosphere Dynamics*. Geological Society, London, Memoirs, **32**, 1–9. http://doi.org/10.1144/GSL.MEM.2006.032.01.01

Gerasimov, M. E., Bondarchuk, G. K., Yudin, V. V. & Beletsky, S. V. 2008. Geodynamic, tectonic zoning the Azov-Black Sea Region. *In*: Khain, V. E. & Gerasimov, M. E. (eds) *Geodynamics, Tectonics and Fluid Dynamics of Oil- and Gas-Bearing Region of Ukraine*. Collection of Reports at the 7th International Conference 'Crimea 2007', 10–16 September 2007, Crimea, Publishing House Forma, Simferopol, 115–151 [in Russian].

Gobarenko, V., Yegorova, T. & Stephenson, R. 2015. Local tomography model of the northeast Black Sea: intraplate crustal underthrusting. *In*: Sosson, M., Stephenson, R. A. & Adamia, S. A. (eds) *Tectonic Evolution of the Eastern Black Sea and Caucasus*. Geological Society, London, Special Publications, **428**, first published on October 27, 2015, http://doi.org/10.1144/SP428.2

Gozhyk, P. F., Chebanenko, I. I. *et al.* 2006. *Objects of Ukraine Perspective for Oil and Gas. Scientific and Practical Grounds of Hydrocarbon Searches in the Azov Sea*. EKMO Publishing House, Kiev [in Ukrainian].

Gozhyk, P. F., Maslun, N. V. *et al.* 2011. Stratigraphic structure of Cenozoic deposits of pre-Kerch Shelf and East Black Sea Basin. *Search and Discovery Article # 5039*.

Grad, M., Guterch, A. *et al.* 2006. Lithospheric structure beneath trans-Carpathian transect from Precambrian platform to Pannonian Basin: CELEBRATION 2000 seismic profile CEL05. *Journal of Geophysical Research*, **111**, B03301, http://doi.org/10.1029/2005JB003647

Grad, M., Guterch, A. *et al.* 2008. Lithospheric structure of the Bohemian Massif and adjacent Variscan belt in central Europe based on profile S01 from the SUDETES 2003 experiment. *Journal of Geophysical Research*, **113**, B10304, http://doi.org/10.1029/2007JB005497

Hippolyte, J.-C., Müller, C. *et al.* 2010. Dating of the Black Sea Basin: new nannoplankton ages from its inverted margin in the Central Pontides (Turkey). *In*: Sosson, M., Kaymakci, N., Stephenson, R. A., Bergerat, F. & Starostenko, V. (eds) *Sedimentary Basin Tectonics from the Black Sea and Caucasus to the Arabian Platform*. Geological Society, London, Special Publications, **340**, 113–136, http://doi.org/10.1144/SP340.7

Janik, T., Yliniemi, J. *et al.* 2002. Crustal structure across the TESZ along POLONAISE' 97 seismic profile P2 in NW Poland. *Tectonophysics*, **360**, 129–152.

KERIMOV, I. A. 2004. *A Method of F-approximations in Solving Direct Problems of Gravimetry and Magnetometry*. Thesis for the degree of doctor in physical-mathematical sciences, United Schmidt Institute of Physics of the Earth, Russian Academy of Sciences [in Russian].

KHAIN, V. E., POPKOV, B. I. *ET AL.* 2009. Tectonics of the southern surroundings of the East European Platform. *In*: KHAIN, V. E. & POPKOV, V. I. (eds) *Explanatory Note for the Tectonic Map of the Black Sea-Caspian Region. Scale 1:2 500 000*. Kuban State University, Krasnodar [in Russian].

KHORTOV, A. V. & NEPROCHNOV, Yu. P. 2006. Deep structure and selected aspects of oil and gas potential of the southern seas of Russia. *Oceanology*, **46**, 105–113.

KHRIACHTCHEVSKAIA, O., STOVBA, S. & STEPHENSON, R. 2010. Cretaceous–Neogene tectonic evolution of the northern margin of the Black Sea from seismic reflection data and tectonic subsidence analysis. *In*: SOSSON, M., KAYMAKCI, N., STEPHENSON, R. A., BERGERAT, F. & STAROSTENKO, V. (eds) *Sedimentary Basin Tectonics from the Black Sea and Caucasus to the Arabian Platform*. Geological Society, London, Special Publications, **340**, 137–157, http://doi.org/10.1144/SP340.8

KOMMINAHO, K. 1998. *Software Manual for Programs MODEL and XRAYS: a Graphical Interface for SEIS83 Program Package*. University of Oulu, Department of Geophysics Report **20**.

KRUGLOV, S. S. & GURSKY, D. S. (eds) 2007. *Tectonic Map of Ukraine. Scale 1:1 000 000*. UkrDGRI, Kiev [in Ukrainian].

LYNGSIE, S. B., THYBO, H. & LANG, R. 2007. Rifting and lower crustal reflectivity: a case study of the intracratonic Dniepr-Donets rift zone, Ukraine. *Journal of Geophysical Research*, **112**, B12402, http://doi.org/12410.11029/12006JB004795

MAYSTRENKO, Yu., STOVBA, S. *ET AL.* 2003. Crustal-scale pop-up structure in cratonic lithosphere: DOBRE deep seismic reflection study of the Donbas Foldbelt, Ukraine. *Geology*, **31**, 733–736.

MOSKALENKO, V. N. & MALOVITSKY, Ya. P. 1974. The results of deep seismic sounding in the transmeridional profile through the Azov and Black Sea. *Izvestia of the Academy of Sciences of the USSR. Geological Series*, **9**, 23–31 [in Russian].

NIKISHIN, A. M. & PETROV, E. I. 2013. *Project Geology Without Limits: New set of seismic data for Black Sea*. http://www.blackseandcaspian.com/…/6-Nikishin-Petr

NIKISHIN, A. M., KOROTAEV, M. *ET AL.* 2003. The Black Sea basin: tectonic history and Neogene–Quaternary rapid subsidence modelling. *Sedimentary Geology*, **156**, 149–168.

NIKISHIN, A. M., ZIEGLER, P. *ET AL.* 2011. Late Palaeozoic to Cenozoic evolution of the Black Sea-southern eastern Europe region: a view from the Russian Platform. *Turkish Journal of Earth Sciences*, **20**, 571–634.

NIKISHIN, A. M., OKAY, A. I. *ET AL.* 2015*a*.The Black Sea basins structure and history: new model based on new deep penetration regional seismic data. Part 1: basins structure and fill. *Marine and Petroleum Geology*, **59**, 638–655.

NIKISHIN, A. M., OKAY, A. I. *ET AL.* 2015*b*. The Black Sea basins structure and history: new model based on new deep penetration regional seismic data. Part 2: tectonic history and paleogeography. *Marine and Petroleum Geology*, **59**, 656–670.

OKAY, A. I., SENGOR, A. M. C. & GÖRÜR, N. 1994. Kinematic history of the opening of the Black Sea and its effect on the surrounding regions. *Geology*, **22**, 267–270.

PANINA, I. V. 2009. Modern structural pattern of the Scythian Plate. *Moscow University Bulletin*, **64**, 21–28.

ROBINSON, A. G., BANKS, C. J., RUTHERFORD, M. M. & HIRST, J. P. P. 1995. Stratigraphic and structural development of the Eastern Pontides, Turkey. *Journal of the Geological Society*, **152**, 861–872, http://doi.org/10.1144/gsjgs.152.5.0861

ROBINSON, A. G., RUDAT, J. H. *ET AL.* 1996. Petroleum geology of the Black Sea. *Marine and Petroleum Geology*, **13**, 195–223.

SAINTOT, A., STEPHENSON, R. A. *ET AL.* 2006*a*. The evolution of the southern margin of Eastern Europe (Eastern European and Scythian platforms) from the latest Precambrian–Early Palaeozoic to the Early Cretaceous. *In*: GEE, D. G. & STEPHENSON, R. A. (eds) *European Lithosphere Dynamics*. Geological Society, London, Memoirs, **32**, 481–505, http://doi.org/10.1144/GSL.MEM.2006.032.01.30

SAINTOT, A., BRUNET, M.-F. *ET AL.* 2006*b*. The Mesozoic–Cenozoic tectonic evolution of the Greater Caucasus. *In*: GEE, D. G. & STEPHENSON, R. A. (eds) *European Lithosphere Dynamics*. Geological Society, London, Memoirs, **32**, 277–289, http://doi.org/10.1144/GSL.MEM.2006.032.01.16

SCOTT, C. L. 2009. *Formation and Evolution of the Eastern Black Sea Basin: Constraints from Wide-Angle Seismic Data*. PhD thesis, School of Ocean and Earth Sciences, University of Southampton.

SHILLINGTON, D. J., WHITE, N. *ET AL.* 2008. Cenozoic evolution of the Eastern Black Sea: a test of depth-dependent stretching models. *Earth and Planetary Science Letters*, **265**, 360–378.

SOLLOGUB, V. B. (ed.) 1987. *Geology of the UkSSR shelf. Tectonics*. Naukova Dumka, Kiev [in Russian].

SPADINI, G., ROBINSON, A. & CLOETINGH, S. 1996. Western versus Black Sea tectonic evolution: pre- rift lithospheric controls on basin formation. *Tectonophysics*, **266**, 139–154.

ŚRODA, P., CZUBA, W. *ET AL.* 2006. Crustal structure of the Western Carpathians from CELEBRATION 2000 profiles CEL01 and CEL04: seismic models and geological implication. *Geophysical Journal International*, **167**, 737–760.

STAROSTENKO, V. I., BURYANOV, V. *ET AL.* 2004. Topography of the crust-mantle boundary beneath the Black Sea Basin. *Tectonophysics*, **381**, 211–233.

STAROSTENKO, V. I., DOLMAZ, M. N. *ET AL.* 2014. Thermal structure of the crust in the Black Sea: comparative analysis of magnetic and heat flow data. *Marine Geophysical Research*, **35**, 345–359, http://doi.org/10.1007/s11001-014-9224-x

STAROSTENKO, V. I., JANIK, T. *ET AL.* 2015*a*. Seismic model of the crust and upper mantle in the Scythian Platform: the DOBRE-5 profile across the northwestern Black Sea and the Crimean Peninsula. *Geophysical Journal International*, **201**, 406–428, http://doi.org/10.1093/gji/ggv018

STAROSTENKO, V. I., RUSAKOV, O. M. *ET AL.* 2015*b*. Heterogeneous structure of the lithosphere in the Black Sea from a multidisciplinary analysis of geophysical fields. *Geophysical Journal*, **37**, 3–28.

STEPHENSON, R. A. & SCHELLART, W. P. 2010. The Black Sea back-arc basin: insight to its origin from geodynamic models of modern analogues. *In*: SOSSON, M., KAYMAKCI, N., STEPHENSON, R. A., BERGERAT, F. & STAROSTENKO, V. (eds) *Sedimentary Basin Tectonics from the Black Sea and Caucasus to the Arabian Platform*. Geological Society, London, Special Publications, **340**, 11–21, http://doi.org/10.1144/SP340.2

STEPHENSON, R. A., MART, Y. *ET AL.* 2004. TRANSMED transect VIII: eastern European Craton-Crimea-Black Sea-Anatolia-Cyprus-Levant Sea-Sinai-Red Sea. Part Two – CD-ROM. *In*: CAVAZZA, W., ROURE, F., SPAKMAN, W., STAMPFLI, G. M. & ZIEGLER, P. A. (eds) *The TRANSMED Atlas: The Mediterranean Region from Crust to Mantle; Geological and Geophysical Framework of the Mediterranean and the Surrounding Areas*. Springer, Berlin, 141.

STEPHENSON, R. A., YEGOROVA, T. *ET AL.* 2006. Late Palaeozoic intra- and pericratonic basins on the East European Craton and its margins. *In*: GEE, D. G. & STEPHENSON, R. A. (eds) *European Lithosphere Dynamics*. Geological Society, London, Memoirs, **32**, 463–479, http://doi.org/10.1144/GSL.MEM.2006.032.01.29

STOVBA, S. & KHRIACHTCHEVSKAIA, O. 2011. Driving and triggering mechanisms of inversion tectonics in the Ukrainian Black Sea. *In*: *3rd International Symposium on the Geology of the Black Sea Region*, 1–10 October 2011, Bucharest, Romania, Abstracts. Geo-Eco-Mar (Suppl), **17**, 177–179.

STOVBA, S. M. & STEPHENSON, R. A. 1999. The Donbas Foldbelt: its relationships with the uninverted Donets segment of the Dniepr-Donets Basin, Ukraine. *Tectonophysics*, **313**, 59–83.

STOVBA, S., KHRIACHTCHEVSKAIA, O. & POPADYUK, I. 2009. Hydrocarbon-bearing areas in the eastern part of the Ukrainian Black Sea. *The Leading Edge*, **28**, 1042–1045.

SYDORENKO, G., STEPHENSON, R. *ET AL.* In prep. Geological structure of the northern eastern Black Sea from regional seismic reflection data, including the DOBRE-2 CDP profile. *In*: SOSSON, M., STEPHENSON, R. A. & ADAMIA, S. A. (eds) *Tectonic Evolution of the Eastern Black Sea and Caucasus*. Geological Society, London, Special Publications, **428**.

TSIOKHA, O., SYDORENKO, G., VOIZIZKY, Z. & POBEDASH, M. 2008. *Regional Geophysical Researches Along the DOBRE-2 Profile*. Report of the State Geophysical Enterprise 'Ukrgeofizika' [in Ukrainian].

ULANOVSKAIA, T. E., ZELENSHCHIKOV, G. V. & KALININ, V. V. 2011. On some unsolved tasks in stratigraphy of the South Eastern Europe. *In*: *Present-Day State of the Art in the Earth Sciences*. Materials of the International Conference in Memory of V.E. Khain, 1–4 February 2011, Moscow. Geological Faculty, Moscow State University, 1920–1926 [in Russian].

VINCENT, S. J., ALLEN, M. B. *ET AL.* 2005. Insights from the Talysh of Azerbaijan in to the Paleogene evolution of the South Caspian region. *GSA Bulletin*, **117**, 1513–1533.

WESSEL, P. & SMITH, W. H. F. 1995. New version of the generic mapping tools released. *Eos*, **76**, 329.

YEGOROVA, T., BARANOVA, E. & OMELCHENKO, V. 2010. The crustal structure of the Black Sea from the reinterpretation of deep seismic sounding data acquired in the 1960s. *In*: SOSSON, M., KAYMAKCI, N., STEPHENSON, R. A., BERGERAT, F. & STAROSTENKO, V. (eds) *Sedimentary Basin Tectonics from the Black Sea and Caucasus to the Arabian Platform*. Geological Society, London, Special Publications, **340**, 43–56, http://doi.org/10.1144/SP340.4

YEGOROVA, T., GOBARENKO, V. & YANOVSKAYA, T. 2013. Lithosphere structure of the Black Sea from 3-D gravity analysis and seismic tomography. *Geophysical Journal International*, **193**, 287–303.

ZELT, C. A. 1994. *Software Package ZPLOT*. Bullard Laboratories, University of Cambridge.

ZONENSHAIN, L. P. & LE PICHON, X. 1986. Deep basins of the Black Sea and Caspian Sea as remnants of Mesozoic back-arc basins. *Tectonophysics*, **123**, 181–211.